Noise properties of a corner-cube Michelson interferometer LWIR hyperspectral imager

D. Bergstrom*[a], I. Renhorn[a], T. Svensson[a], R. Persson[a], T. Hallberg[a], R. Lindell[a] and G. Boreman[b]
[a]FOI – Swedish Defence Research Agency, P.O. Box 1165, SE-581 11 Linkoping, Sweden
[b]University of Central Florida, CREOL/College of Optics & Photonics, Orlando, FL 32816-2700, USA

ABSTRACT

Interferometric hyperspectral imagers using infrared focal plane array (FPA) sensors have received increasing interest within the field of security and defence. Setups are commonly based upon either the Sagnac or the Michelson configuration, where the former is usually preferred due to its mechanical robustness. However, the Michelson configuration shows advantages in larger FOV due to better vignetting performance and improved signal-to-noise ratio and cost reduction due to relaxation of beamsplitter specifications. Recently, a laboratory prototype of a more robust and easy-to-align corner-cube Michelson hyperspectral imager has been demonstrated. The prototype is based upon an uncooled bolometric FPA in the LWIR (8-14 μm) spectral band and in this paper the noise properties of this hyperspectral imager are discussed.

Keywords: hyperspectral imager, Michelson interferometer, LWIR, uncooled bolometer, noise, NESR, SNR

1. INTRODUCTION

Hyperspectral imaging (HSI) is receiving a continued growth of interest from defence, civil, commercial as well as scientific communities, as adding a spectral dimension to imaging can be beneficial for a range of applications. HSI is used in monitoring health of plants in agriculture and identifying minerals in geological surveys, as the spectral signature of objects works as fingerprints in identifying the materials they are composed of. In military surveillance, HSI offers more advanced and robust detection capabilities as hiding or camouflage measures in specific spectral bands become more difficult as the number of monitored bands increases.

The method of extracting the spectral information separates the different hyperspectral imagers into filtering, dispersive and interferometric instruments. The preferred solution depends on performance requirements. In the present realisation, low cost is emphasized at the expense of SNR performance. Since the optics will be uncooled and the sensor requires rather high signal levels, an interferometric solution is selected.

Interferometric setups are usually based upon either the Sagnac or the Michelson configuration, where the former is usually preferred due to the absence of movable components and its mechanical robustness. However, the Michelson configuration shows advantages in larger field-of-view (FOV) due to better vignetting performance because of the shorter optical path. Moreover, due to the fact that the two interfering beams of the Michelson design pass the beamsplitter once in transmission and once in reflection, while in the Sagnac design one beam passes twice in transmission and the other twice in reflection, the Michelson design is less sensitive to the reflection and transmission variations of the beamsplitter. This offers improved fringe contrast in the interferogram over a larger spectral range and therefore higher signal-to-noise ratios (SNR) as well as a cost reduction in the design.

In the traditional Michelson configuration, both the fixed and movable mirrors are plane and therefore sensitive to tilt. Corner-cube interferometers have been investigated in various contexts, with their appeal stemming from the angular insensitivity of the corner cubes resulting in relaxed alignment tolerances. The imaging capabilities of a lab prototype of a hyperspectral imager, based on a Michelson corner-cube configuration and an uncooled bolometric FPA in the LWIR 8-14 μm band, was recently demonstrated[1]. In this paper, the noise properties of the instrument are discussed.

*a david.bergstrom@foi.se; phone: +46 13 378226, fax: +46 13 378066, www.foi.se

Infrared Technology and Applications XXXVI, edited by Bjørn F. Andresen, Gabor F. Fulop, Paul R. Norton,
Proc. of SPIE Vol. 7660, 76602F · © 2010 SPIE · CCC code: 0277-786X/10/$18 · doi: 10.1117/12.851433

2. INSTRUMENT SETUP

The laboratory setup, see principal sketch and photo in Fig. 1, is based on a standard Michelson interferometer, but with the two plane mirrors substituted with two gold-coated front-surface corner-cube reflectors, of 63.5-mm diameter. The corner-cubes, purchased from Edmund Scientific, have a specified retroreflection parallelism of 1 arc second (~ 5 μrad). The relative horizontal position offset between the corner cubes was varied between 0.75 and 3.0mm.

The beamsplitter and a nominally identical compensator plate were made from ZnSe and were purchased from II-VI Infrared. Both were in rectangular format 70 mm × 100 mm × 7 mm. One surface of the beamsplitter was a nominal 50/50 LWIR beamsplitter coating, while the other surface (and those of the compensator) were coated with a broadband antireflector, with less than 1% reflection across the 8-14 μm band. The two ZnSe plates were mounted together, separated by metallic shims of about 50 μm thickness, with the beamsplitter coating on an interior surface. It was found that the compensator plate was critical in obtaining high-contrast fringes from the thermal source due to spectral dispersion.

The IR camera was a Miricle 307K model, supplied by Thermoteknix, which is a bolometric uncooled focal plane array (FPA) in a 640 × 480 format with a spectral response between 7 and 14 μm. The bolometer is an amorphous silicon FPA, manufactured by ULIS, with a 25 μm pixel pitch and a fill factor of about 80%. The f/1 camera lens was a Germanium lens, with a 50-mm focal length and which was focused at infinity. With this lens, the nominal noise-equivalent temperature difference (NETD) was 85 mK. The total dynamic range for output data was 14 bits. The object used was a freestanding film of polypropylene, backlit by an 86°C extended-area blackbody source (SR-80 from CI Systems) of 10 cm^2 area. With this setup, useful interference fringes were obtained nearly to the edge of the FOV.

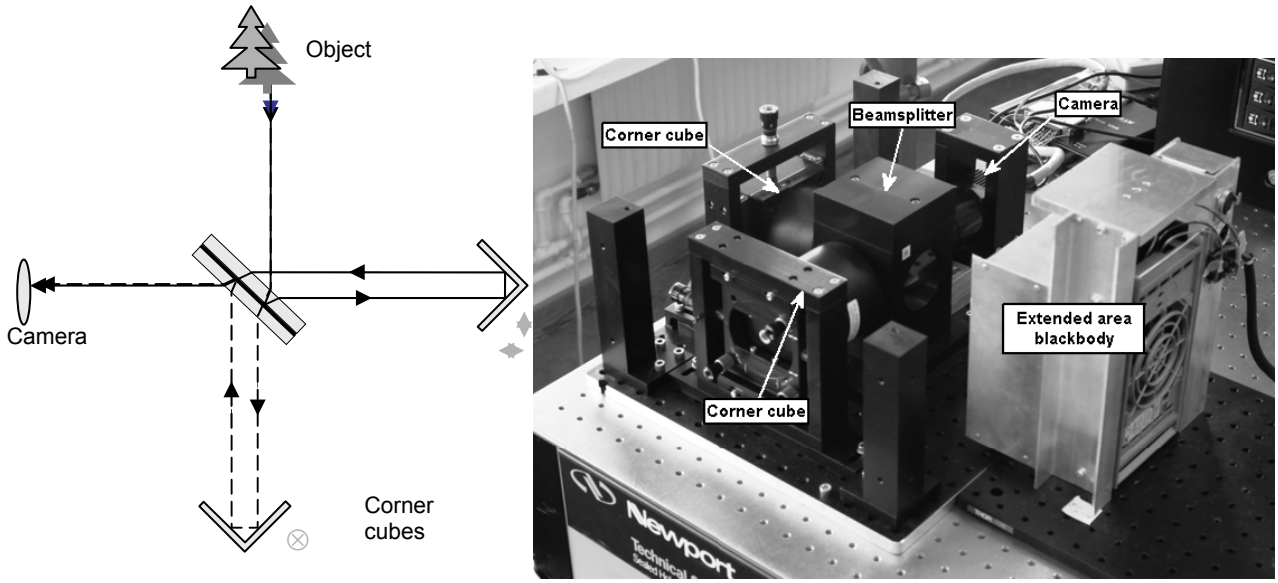

Figure 1. Left: Principal sketch of the interferometer setup. The beam splitter and compensator plate are both fixed, mounted in the rigid construction with a space of 50 μm. The corner cube to the right is adjustable in X and Y while the corner cube at bottom is adjustable in Z direction (the corner cubes in the figure are shown in only 2 dimensions). Right: Photo of the instrument setup, with an extended area blackbody placed in the object plane.

3. THEORY

2.1 Fringe shaping and spectral resolution limits

In the imaging Michelson interferometer, fringes are obtained by slightly off-setting one of the corner-cubes and by using the varying angle of incidence from the scene. Constant fringe spacing as a function of angle is determined by the

off-set magnitude. The spectral resolution can therefore be conveniently varied by adjusting the relative position of the corner cubes. Two advantages compared to the Sagnac interferometer are obvious. First, the instrument can be made more compact with smaller vignetting. Second, small imbalances in the beamsplitter nominal 50/50 splitting ratio are not decreasing the fringe contrast as in the Sagnac interferometer.

Each pixel corresponds to an angular deviation that is determined by the focal length and the pixel pitch. For the present camera, the nominal value is $\Delta\theta$=0.5 mrad per pixel. The optical path difference is determined by the beam off-set, Δx, which is twice the corner-cube offset and the angular deviation. The optical path difference (OPD) is given by

$$OPD=\Delta\theta\ \Delta x\ (n-n_c), \quad (1)$$

where n_c is the pixel number of the centered interferogram.

The Nyquist wavelength is given by $2OPD_{Min}$ or $2\Delta\theta\Delta x$. If radiation from sources with spectral content shorter than the Nyquist wavelength is detected, aliasing will be observed. Since the bolometer has spectral response down to 7 μm, the maximum beam offset allowed before folding degrades spectral data will therefore be Δx_{max}=0.70 cm. This Δx_{max} will then determine the highest spectral resolution attainable with the current instrument design.

The spectral resolution is given in wavenumbers by

$$\Delta\sigma=1/OPD_{Max} \quad (2)$$

and in wavelength by

$$\Delta\lambda=\lambda^2/OPD_{Max}, \quad (3)$$

where OPD_{Max}=2OPD (± OPD) with OPD as defined in Eq. (1).

The highest spectral resolution is therefore calculated as 2.2 cm^{-1} and 4.5 cm^{-1} for single- and double-sided interferograms, respectively. In wavelength units this corresponds to 0.022 μm (single-sided) and 0.045 μm (double-sided) for λ=10 μm. Vignetting effects and noise will in practise determine the resolution before these limits are reached.

2.2 Noise sources and figures of merit

Sources of noise in FT-IR measurements can broadly be categorized into noise independent of source intensity, such as detector noise (1/f, Johnson, thermal fluctuation and read-out noise being dominant for microbolometers), noise proportional to the square root of source intensity, e.g. photon shot noise, and noise proportional to intensity, e.g. source/scene fluctuation noise[2-6]. For a fielded instrument, additional platform related noise sources can also contribute, e.g. vibrations causing optical jitter, as well as atmospheric effects like scintillation and turbulence.

Generally, the signal to noise ratio (SNR) of an interferometric spectrometer depends on both sensor parameters and spectral properties. Uncooled bolometer sensors are limited by detector noise and are therefore independent of the level of radiation. Noise will be added from each independent spectral channel, i.e. the noise is determined by the sensor noise that for uncorrelated measurements also is related to the spectral channel noise. Using the complex Fourier transform in order to obtain the spectrum from a two-sided interferogram, both the signal and the noise standard deviation will be divided by two. Noise will also cause a spectral bias. If noise is assumed to be normally distributed, the bias will be $\sqrt{2/\pi}\rho$, where ρ is the RMS noise. If the noise level can be determined, this bias might be subtracted from the spectrum.

A common figure of merit for the sensitivity of an FT-IR imaging spectrometer is the noise equivalent spectral radiance (NESR), usually given in units of [W/cm^2/sr/cm^{-1}], which is the change in radiance at the sensor's aperture equal to the system noise within a specified spectral band. Theoretically it can be calculated from[7]

$$\text{NESR} = \text{NEP} / (0.5\ \tau\ \text{M}\ \Theta\ \Delta\sigma\sqrt{t}\ ), \tag{4}$$

where NEP is the noise equivalent power, τ is the instrument transmission efficiency, M is the beamsplitter modulation efficiency, Θ is the single pixel throughput, $\Delta\sigma$ is the spectral resolution and t is the measurement time. The NEP is given by the root sum square of all the noise contributions. For detector-noise limited spectrometers NEP = $\sqrt{A_D B} / D^*$, where A_D is the detector area, B is the effective noise bandwidth and D^* is the specific detectivity of the detector.

Experimentally, the NESR is usually calculated as the 1-sigma noise of the detector calibrated to a spectral radiance using a blackbody reference[8]. The signal-to-noise ratio (SNR) is then simply given by the ratio of the measured spectral radiance to the NESR in the specific spectral band, e.g.

$$\text{SNR} = \frac{L(\sigma_i)}{NESR(\sigma_i)}. \tag{5}$$

For a spatially modulated Fourier transform spectrometer, non-uniformity correction of fixed pattern noise and bad pixel identification and filtering must be included to reduce spatial noise which otherwise will further degrade the SNR performance of the instrument.

4. RESULTS

In Figure 2, a full-FOV image of an 86°C extended area blackbody source (SR-80 from CI Systems) is shown with an averaged interferogram calculated from a centered 100-line section across all FPA columns shown on the left. In Figure 3, an image of a polypropylene film backlit by the same blackbody source is shown, with its associated averaged interferogram on the right. In both cases, the corner-cube offset was 1.5 mm, corresponding to a spectral resolution of 20.8 cm^{-1}. Some vignetting can be seen, as the fringe contrast is reduced from the center zone of the FPA, but for the polypropylene film fringes can be seen almost to the edge of the detector.

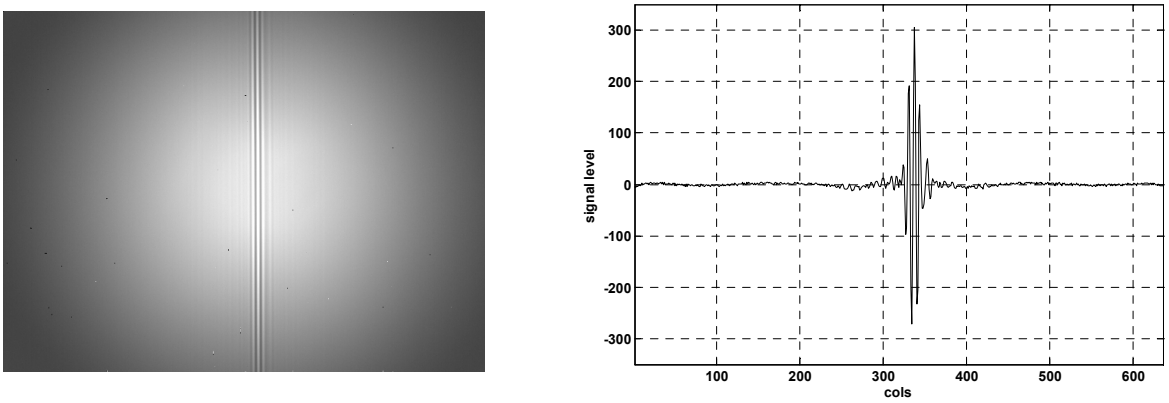

Figure 2. Full-FOV image of a 86°C blackbody source (left) with the associated interferogram (right).

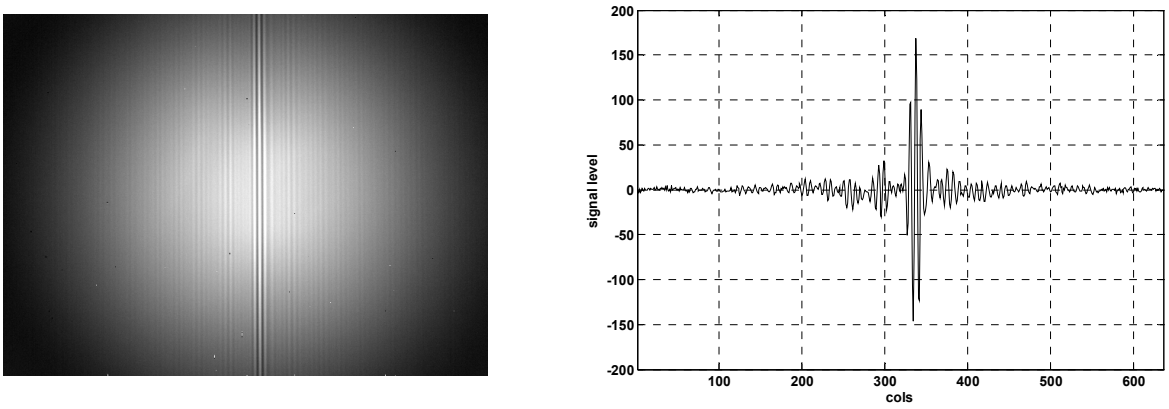

Figure 3. Full-FOV image of a polypropylene film backlit by a 86°C blackbody source (left) with the associated interferogram (right).

4.1 Transmittance measurements

In Figure 4, a measured transmittance spectrum for three different spectral resolutions is shown for the polypropylene film. The spectral resolutions are 20.8 cm^{-1}, 10.4 cm^{-1} and 5.2 cm^{-1}, corresponding to 0.075 cm, 0.15 cm and 0.3 cm corner-cube offsets, respectively. Data records are typically obtained as 400 frame sequences, with a frame rate of 60Hz. A camera-specific non-uniformity correction was performed prior to data collection. To increase the SNR, the individual frames of data are averaged together and the median of about 20 central rows is used for the calculation of the interferogram. A 6^{th}-order polynomial is fitted and subtracted from the interferogram for baseline correction. Apodization is performed by applying a Hamming window to the whole length of the data set and the power spectrum is then calculated using an FFT with zero-filling applied for spectral interpolation. The spectrum of the blackbody plus film is divided by the spectrum of the blackbody only to yield the transmittance spectrum of the film.

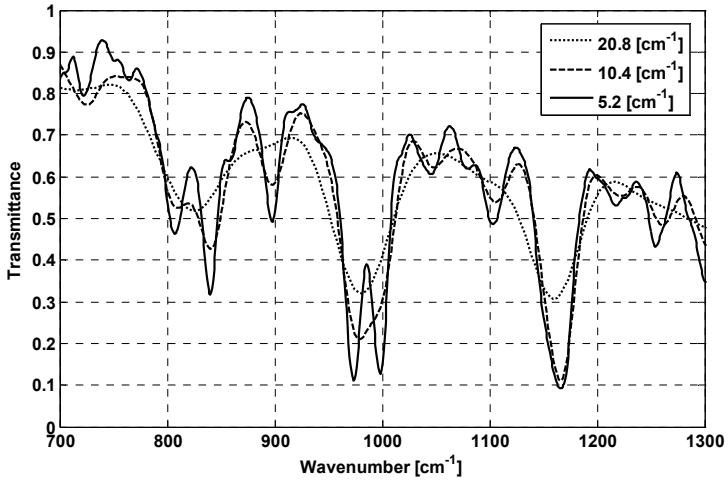

Figure 4. Measured transmittance spectra for a polypropylene film for three different spectral resolutions.

4.2 Temporal NESR and SNR measurements

Temporal NESR measurements of the instrument were performed for three spectral resolutions by calibrating a 400 frame observation of an extended area blackbody at 86°C to spectral radiance and computing the standard deviation, yielding the spectral curves as seen in Figure 5. To limit the effects of vignetting, the NESR measurements were made

for each pixel in the central 100 rows of the detector and then averaged. Bad pixels were also removed from the group. It can be seen that the NESR is reasonably flat between 900 cm-1 and 1200 cm-1, but increases for lower wavenumbers, which could be the result of reduction of beamsplitter efficiency, lens transmission and detector response. For higher wavenumbers there is also a modest increase, expected to arise from the short wavelength limit of the α-Si bolometer response and the modulation transfer function (MTF) of the optics at higher spatial frequencies[9].

The SNR was computed by taking the mean value of the measured spectral radiance of the blackbody divided by the NESR and the results in Figure 6 show that the $SNR \propto \Delta\sigma$, in accordance with Eq. (4).

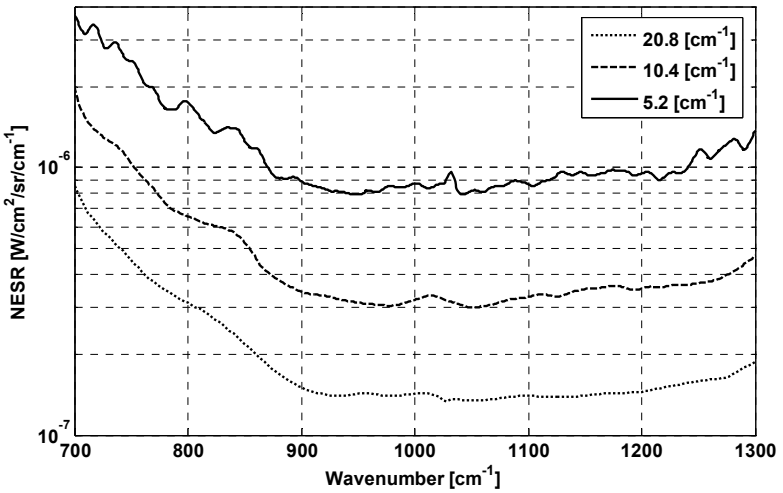

Figure 5. Noise equivalent spectral radiance (NESR) for three different resolutions.

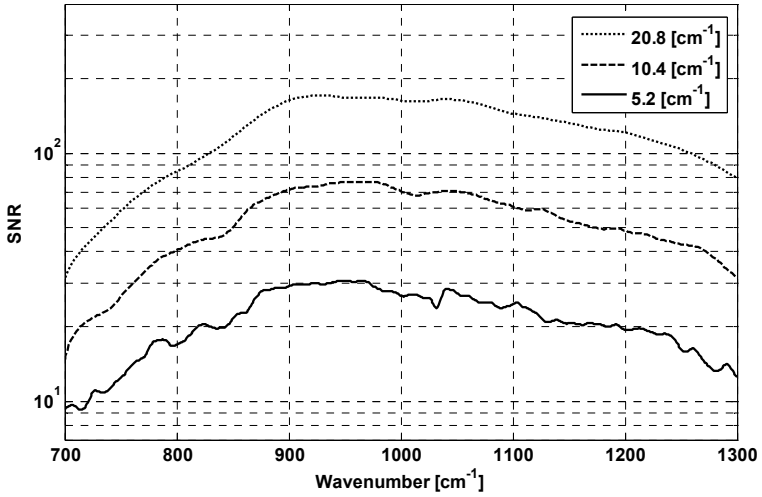

Figure 6. Signal-to-noise ratios (SNR) for three different resolutions.

5. DISCUSSION

Interferometric spectrometers based on uncooled imaging sensor technologies have the potential to be useful low cost instruments in the thermal infrared spectral region. The advantage of using a Michelson design and corner-cubes with offset has been demonstrated. Although vignetting is substantial in the present design, useful interference data are obtained nearly to the edges of the images.

The SNR can be further increased by improving the optical design. Additional improvements in uncooled sensor performance can also be expected. It was also noted that spatial noise was rather significant in the images analyzed and reduction of this component can be expected to give further improvement. For detector-noise-limited performance, the model according to Lucey *et al*[8] (neglecting the spectral efficiency of the interferometer), the NEP can be written as

$$\mathrm{NEP} = \mathrm{NEDT}\,\frac{\tau_0 A_D\,\Delta P/\Delta T}{4f^2+1}, \tag{6}$$

where τ_0 is the transmission of the optics, A_D is pixel area, $\Delta P/\Delta T$ is the change in power with temperature over the wavelength range and f is the focal ratio. The blackbody signal power is given by $P = L_\sigma \Delta\sigma A_D \tau_i$, where L_σ is the blackbody spectral radiance and τ_i is the interferometer transmission. SNR is then the ratio of P and NEP and the result for the input data in Table 1 is shown in Figure 7, showing a potential factor of roughly 1.5 in improvement over most of the spectral range.

Table 1. Model input data.

Parameter	Value
NEDT	85 [mK]
Optics transmission, τ_0	0.95
F-number, f	1.0
Interferometer transmission, τ_i	0.50
Pixel area, A_D	500 [μm^2]
$\Delta P/\Delta T$	2.62x10-4 [W/cm^2K] [8]
Spectral resolution, $\Delta\sigma$	5.4 [cm^{-1}]
Blackbody temperature	359 [K]

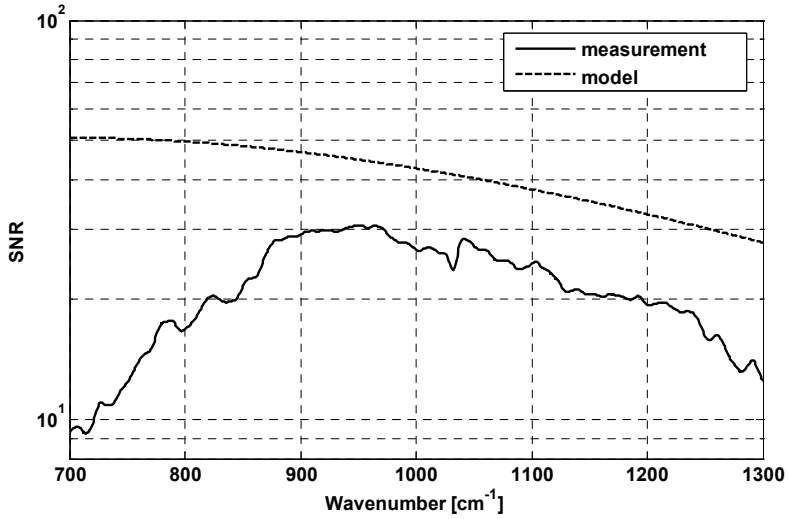

Figure 7. Model (detector noise limited performance) and measurement comparison of the corner-cube Michelson hyperspectral sensor for $\Delta\sigma$=10.4cm^{-1} spectral resolution.

Finally, the spectral capability is demonstrated by comparing transmission of polypropylene with a corresponding reference spectrum. The independent transmittance measurements were performed on a commercial Bruker IFS 55 spectrometer, equipped with a liquid nitrogen cooled MCT detector, with a spectral resolution of 0.5 cm^{-1}. A comparison between the two instruments is shown in Figure 8, for the polypropylene film, showing quite good agreement over most of the spectral range.

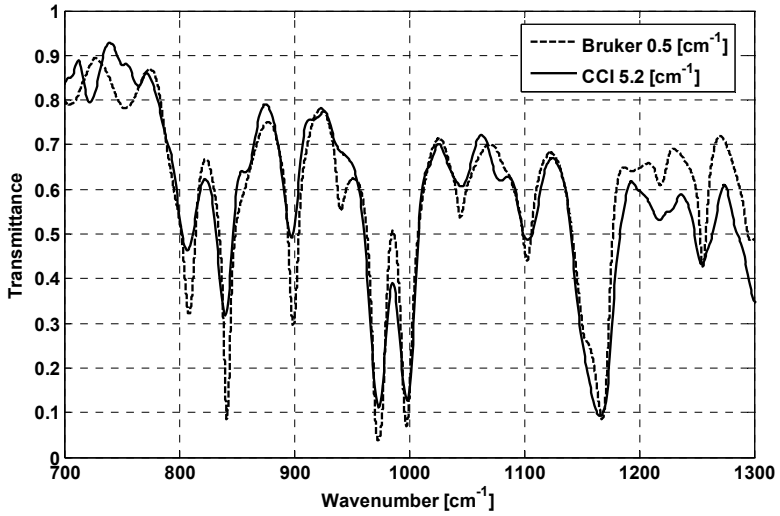

Figure 8. Comparison of transmittance spectra of a polypropylene film, as measured by a Bruker IFS 55 spectrometer and the corner-cube interferometer (CCI).

REFERENCES

1. Renhorn, I. G. E., Svensson, T., Cronstrom, S., Hallberg, T., Persson, R., Lindell, R. and Boreman, G. D., "Demonstration of a corner-cube-interferometer LWIR hyperspectral imager", Infrared, Millimeter and Terahertz waves 31(1), 60-65 (2010).
2. Davis, S. P., Abrams, M. C. and Brault, J. W., [Fourier Transform Spectrometry], Academic Press, 119-141 (2001).
3. Griffiths, P. R. and de Haseth, J. A., [Fourier Transform Infrared Spectrometry], Wiley Interscience, 161-175 (2007).
4. Sellar, R. G. and Boreman, G. D., "Comparison of relative signal-to-noise ratios of different classes of imaging spectrometer", Applied Optics 44(9), 1614-1624 (2005).
5. Niklaus, F., Vieider, C. and Jakobsen, H., "MEMS-based uncooled infrared bolometer arrays – A review", Proc. SPIE 6836, 6836 0D (2008).
6. Liger, M., "Uncooled carbon microbolometer imager", Doctoral Thesis, California Institute of Technology, 33-41 (2006).
7. Harig, R., "Passive remote sensing of pollutant clouds by FTIR spectrometry: Signal-to-noise ratio as a function of spectral resolution", Applied Optics 43(23), 4603-4610 (2004).
8. Lucey, P. G., Horton, K. A. And Williams, T., "Performance of a long-wave infrared hyperspectral imager using a Sagnac interferometer and an uncooled microbolometer array", Applied Optics 47(28), F107-113 (2008).
9. Sellar, R. G. and Rafert, J. B., "Effects of aberrations on spatially modulated Fourier Transform Spectrometers", Optical Engineering 33(9), 3087-3092 (1994).